International Journal of Research
Available at https://edupediapublications.org/journals
p-ISSN: 2348-6848
e-ISSN: 2348-795X
Volume 06 Issue 13
December 2019

PV Battery Charger Using an *L3C* Resonant Converter for Electric Vehicle

Gadige Shivakumar[1]. Muthvala Sridhar[2]. Dr.A.Mallikariuna Prasad[3]
[1]P.G. Scholar, [2]Guide, Assistant Professor, [3]Head of the Department
[1,2,3] Branch :EEE (Power And Industrial Drives)
[1,2,3] Geethanjali College of Engineering and Technology Nannur.
Email id : [1]g.shivakumar6876@gmail.com, [2]sridharmuthyala@gmail.com

ABSTRACT
In Electric Vehicles with rooftop PV panels, the solar irradiance and surface temperature can affect their performance and output voltages (e.g., V_{pv} = 24−45VDC). In these systems, the maximum energy must be extracted from the variable input voltage (PV panel), boosted by different gains, and stored in high voltage battery packs. Furthermore, depending on the battery state of charge, the charger should operate in constant voltage, constant current, or constant power modes, all the way from complete discharge condition, up to the charged floating voltage phase (V_{bat} = 230 − 430VDC).

This combination of the variable PV input voltage and different states of charge creates a significant regulation challenge for the converter. In this paper, a high efficiency fourth orderL3C resonant converter is proposed with an extreme voltage regulation capability that can effectively extract the maximumpower from the PV panels and respond to the battery states of charge at different voltage and current levels. The experimental results from a 350W prototype prove the features of the proposed L3C resonant converter and demonstrate its ability to track the maximum input power while responding to the battery various states of charge.

Keywords:- Batteries, Voltage control, Inductance, Temperature, Topology, State of charge

INTRODUCTION
DC-DC power converters with variable voltage gain and boosting features are among the main components for PV energy systems, since the maximum power must be extracted from the low voltage, variable input source and boosted to a high voltage level [1, 2]. In PV energy systems for Electric Vehicles (EVs) with rooftop PV panel, it is also essential to employ a rechargeable battery pack to store energy and release it later [3–7]. Using battery packs for energy storage imposes challenging design constraints for the power converter, due to the different battery operating modes, including constant current, constant voltage, constant power, and no-load condition [8]. The combination of a PV panel and are chargeable battery in an energy system requires extreme voltage gain variations from the input (V_{pv} = 24−45VDC) to the output(V_{bat} = 230−430VDC), and this needs to be supported by solar battery chargers. In this case, the charger should not only track the input voltage variation in order to extract the maximum available power from the PV panel, but also boost the input voltage according to the level of variable gain and respond to the battery different states of charge.

Recently, different studies have been dedicated to developing reliable and efficient non-isolated and isolated power converters for PV applications. Non-isolated power converter topologies which have

been used in PV systems include boost converters, Cockcraft-Walton multipliers, coupled inductors, and switched inductors-capacitors with high voltage gain capability as the DC-DC power conversion stage for PV to grid applications(boosts a low, variable input voltage of 30 − 50VDC to a high, fixed output voltage of 400VDC) [9–13]. Although non-isolated power converters can successfully boost the PV voltage and reach high performance, they are not recommended for Electric Vehicle applications that require mandatory galvanic isolation between the PV panel and the high voltage battery pack.

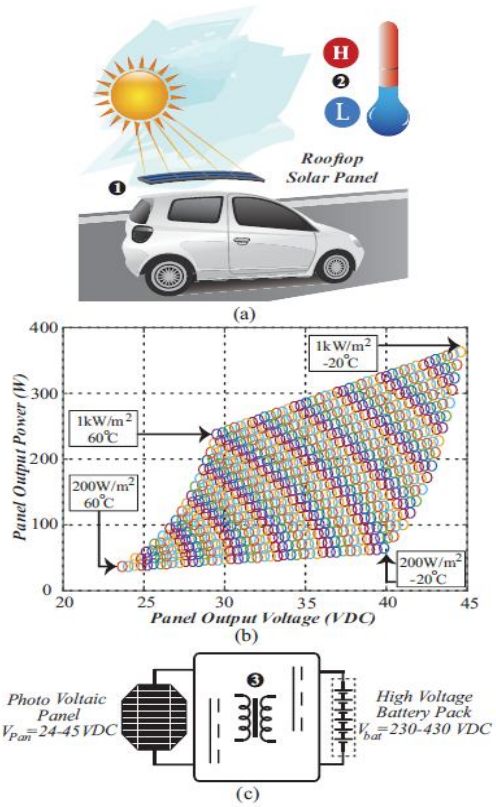

Fig. 1. a) Example of EV with rooftop solar panel subject to changing sun irradiance 1) and temperature 2) , b) PV panel Power-Voltage characteristic covered by the DC-DC converter , and 3) galvanic isolation 3 regulation requirement to supply 230 − 430VDC wide battery voltage from 24 −45VDC PV voltage.

According to safety standards UL60950 and UL1741, isolated applications require at least 4kV galvanic isolation to be provided between the PV panel and the battery pack in order to prevent any high voltage shock path [14, 15]. Among isolated PWM power converter topologies, fly back, current fed push-pull topology, z-source, and Phase-Shift-Full-Bridge power converters have attracted the most attention. These converters can achieve a high step-up gain from transformers with large turn ratios while tracking the input voltage variation by changing the effective duty cycle [16–18].Different improvements such as interleaving, and active clamp circuit have been presented in order to decrease the input current ripple and transfer the maximum input power to the output with soft switching across the main switches [19, 20]. These interesting converters target the maximum energy transfer from a variable input voltage to a fixed output voltage, rather than responding to different voltage and current operating modes of the high voltage battery pack. In particular, storage applications with new battery technologies (e.g., Li-Ion) push the charger output requirements of the PV converter to unprecedented levels. Insightful research on resonant converters has been presented in literature with single and double conversion stages for battery charger or PV applications with fixed input and fixed output voltage, respectively; including current-fed parallel, modified and bidirectional, hybrid, and quasi-Z-source resonant converters [21–28]. These converters successfully handle the PV voltage variations and Maximum Power Point Tracking (MPPT) requirements or respond to different battery states of charge, but do not focus on both input and output variations at the same time. Resonant power converters will be reviewed in detail in Section III in order to present each topology configuration, its application, and the voltage regulation capability. The particular

application, addressed in this paper, involves the challenging scenario of extracting the energy from a variable input voltage source (PV panel) and transferring it to a high voltage battery pack, which needs to be regulated at different current and voltage levels. As an example, Fig. 1(a) shows a single PV panel on the rooftop of an EV. The power capacity range is from 50W to 350W and the input voltage ranges widely from V_{pv} = 24 − 45VDC. This undesirable wide input variations due to the effect of solar irradiance and surface temperature that affects the Power-Voltage characteristics of the PV panel illustrated in Fig. 1(b). As well, the battery pack depicted in Fig.1(c) shows that the output voltage should comply with extreme regulation as well to cover 230 − 430VDC.

This paper proposes a high efficiency, isolated fourth orderL3C resonant converter with extreme regulation capability for PV to high-voltage battery pack applications with the aim of tracking the maximum input power while responding to the battery states of charge at different output voltage and current levels. Incomparison with well-known resonant power converter topologies(e.g. L3C2, LCLC, LCL2, LCC, and LCL), the proposed topology presents a steep voltage gain versus frequency, means lower frequency variation for input-output regulation, which makes it a good candidate for PV to high voltage battery pack applications. Also, the proposed resonant topology has a voltage gain of more than two for the resonant tank, which can be counted as a part of the boost action and reduces the transformer turns ratio and simplifies its structure. Due to its inherent over current capability, the proposed converter can control the charging current during constant current mode or transient conditions; this capability also eliminates the need for an over current and short circuit protection, and facilitates the current control loop design.

Due to operating in the inductive load region, power MOSFETs in the high frequencyL3C resonant converter always work in ZVS for different load conditions, providing high-efficiency, low-noise output voltage. Moreover, The parallel resonant capacitor, put in the secondary of the transformer, leads to Zero Current Switching (ZCS) of the output rectifier diodes, eliminates the voltage peak produced by the diodes reverse recovery current and decreases the noise in theoutput voltage. In this paper, the general equations for solar PV panels will be extracted and employed to determine the variation of Power-Voltage characteristics of a specific PV module versus irradiance and temperature variations.

Then, a detailed review is presented for well-known resonant power converters in order to describe their structures and distinguish the difference between the proposed L3C resonant converter and its features in comparison with other resonant topologies. Later, the complete analysis of the L3C resonant converter with consideration of parasitic elements(including leakage inductances and parasitic capacitances) is obtained. Using the analytical equations extracted for fourthorderL3C resonant circuits, a 350W DC-DC power converter is designed and implemented. Finally, experimental results are presented to demonstrate the circuit performance and to prove the extreme regulation feasibility for both input and output sides. The results show the L3C resonant converter can track all input voltage variations related to maximum input power (V_{pv} = 24 − 45VDCpresented in Fig. 1(b)), while regulating the battery voltage from230VDC to 430VDC.

RESONANT POWER CONVERTERS REVIEW

Softly switched resonant converters are excellent candidates for DC-DC power supply design with wide regulation, due to their capability to produce variable voltage gains in different operating frequencies, while providing soft switching conditions for semiconductor devices [34]. In this section, well-known resonant power converters will be presented in order to review the application of each topology and distinguish the difference between the L3Cresonant circuit and other fourth order ones. Also, this section will present and compare the voltage gain characteristics of each resonant power converter with the proposed L3C. To date, the most complicated resonant power converter contains a fifth order resonant network, including three inductors and two capacitors, as presented in Fig. 4(a). The first application of LCL2C resonant topology was for high voltage DC-DC power supplies, due to its ability to absorb the parasitic capacitor of the transformer with a high turns ratio, also working with a fixed-frequency phase-shift control approach [35].

Another interesting application of LCL2Cis for battery chargers, due to its capability to extend the switching frequency beyond the second resonant frequency and cover nearly all regions required in the battery VI plane [36]. While fifth orderL3C2 resonant converters can regulate the output voltage, a wide switching frequency variation and non-operating area leads to more complicated power and control circuit design. In comparison with fifth order resonant topologies, the fourth order LCLC resonant converter does not take into account the effects of the transformer secondary leakage inductance ($L_{s2} \rightarrow 0$), which leads to a less accurate steady-state analysis and regulation capability [37]. This resonant circuit is presented in Fig. 4(b). Similar to the LCL2Cresonant circuit, LCLC employs the parallel resonant capacitor in its circuit and can be used for high voltage DC-DC applications.

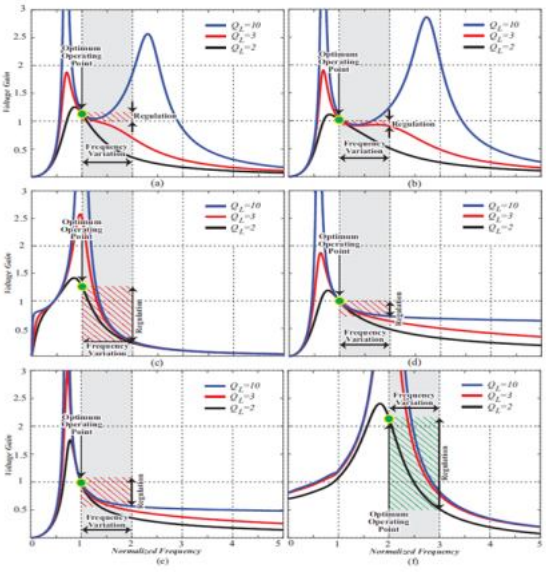

Fig. 5. Voltage gains of different resonant power converters versus normalized switching frequency and constant values of normalized parameters (L_n,L_s, C_n, QL): (a) LCL2C for $L_n = 0.25$ and $L_s = 5$ and $C_n = 0.5$, (b) LCLC for $L_n = 0.25$ and $C_n = 0.5$, (c) LCC for $C_n = 0.5$, (d) LCLfor $L_n = 0.25$, (e) LCL2 for $L_n = 0.25$ and $L_s = 5$, (f) L3C for $L_n = 0.25$ and $L_s = 5$.

Besides, LCLC has two resonant frequencies and is able to extend the switching frequency beyond the second resonant frequency for a better regulation. Both third order LCC and LCL resonant converters are extracted from the LCLC resonant circuit, when $L_p \rightarrow \infty$ or $C_p \rightarrow 0$, respectively. These two third order resonant power converters have been reported in the literature fora variety of applications. The LCC resonant converter has been employed in DC-DC power converters with low voltage and high voltage output level [38, 39]. As shown in Fig.4(a)-(f), this resonant converter has a relatively better regulation

capability in comparison with other well-known resonant converters. Even though the LCL resonant topology has become a popular resonant converter for battery charger and telecom applications, it is well understood that the existence of diode junction capacitances creates limitations for LLC resonant converter in terms of the maximum operating frequency and regulating the input-output voltage in a wide range[8, 40, 41]. In DC-DC power converters with a low output voltage, the transformer parasitic capacitor can be neglected and in Fig. 4(a)with Cp → 0, a higher order model for LCL resonant circuit can be obtained. In fact, the LCL2 resonant converter employs third order model of the transformer, which leads to a more accurate steady state analysis. The research in [42] has proved that theLCL2 resonant converter has steeper voltage gain curves andwider output voltage regulation in comparison to the LCL resonant power converter. Although all of the above-mentioned resonant topologies can to some extent respond to the input voltage variation and operate under MPP, they struggle to attain the required output voltage regulation, which makes them unsuitable for the target application.

The proposed resonant topology presented in this paper can be obtained by removing the series resonant capacitor in Fig. 4(a),Cs →∞. It means that the fourth order L3C can be obtained from the fifth order LCL2C resonant topology if the series resonant capacitor is selected as a DC blocking capacitor or completely eliminated from the circuit. Studying the behavior of the L3Cresonant circuit presented in Fig. 4(f) shows that this topology presents a completely different behavior for the voltage gain versus frequency. In order to compare the regulation capability of the previous resonant power converters and with the proposed one,normalized steady-state equations of each resonant topology are used to draw voltage gains versus normalized frequency. Fig. 5presents resonant converters voltage gains for the same amount of normalized parameters and loaded quality factor, QL. For each resonant converter, the normalized frequency variation is selected to be one and the voltage regulation characteristic is studied. According to the obtained results, L3C and LCLC resonant topologies have the highest and lowest regulation capability among all resonant power converters. In comparison to the resonant converter presented in Fig. 4(a)-(e), the proposed topology presents a steep voltage gain versus frequency, meaning lower frequency variation for input-output regulation. More importantly, all the well known resonant converters present a voltage gain of around one for the optimum operating point, while the proposed L3C topology has a voltage gain of more than two, which makes it an excellent candidate for PV to high-voltage battery pack applications.

Another important advantage of resonant topologies with a parallel resonant capacitor, including LCL2C, LCLC, LLC, andL3C is the ability to provide soft switching conditions for output rectifier in all operating conditions. Fig. 6 shows the schematic of the output rectifier with the parallel resonant capacitor along with its main waveforms. According to Fig. 6, there are two intervals in each switching period that the output rectifier diodes turn off and

International Journal of Research
Available at https://edupediapublications.org/journals
p-ISSN: 2348-6848
e-ISSN: 2348-795X
Volume 06 Issue 13
December 2019

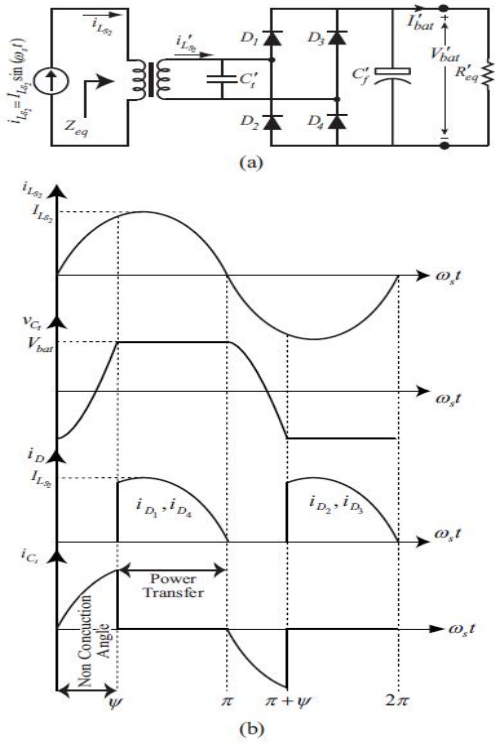

Fig. 6. a) Output rectifier with the parallel resonant capacitor, and b) main waveforms.

the resonant circuit is being disconnected from the load, called on-conduction angle. This off-state interval leads to Zero Current Switching of the diodes and eliminates the noise in the output voltage that is produced by the diodes reverse recovery current [35].Also, due to the semi-sinusoidal waveform of the diode voltage, the diodes turn on and off at low dv/dt and the drawback effect of the diode junction capacitance during transient times can be minimized. Once the voltage across the parallel resonant capacitor reaches tothe output voltage, the rectifier diodes are forward biased and start transferring power to the load. Despite resonant topologies with a parallel resonant capacitor, LCL and LCL2 resonant topologies can only provide soft switching condition for output rectifier diodes when the converter operates at or below short circuit resonant frequency [42, 43].

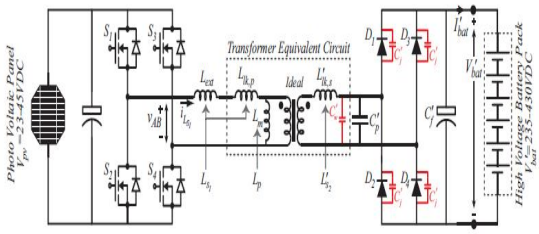

Fig. 7. Full bridge L3C resonant converter schematic with capacitive output filter, applicable for PV to high voltage battery applications.

STEADY STATE ANALYSIS OF L3C RESONANT CONVERTER

Fig. 7 shows a complete schematic of the proposed L3Cresonant converter, including transformer secondary side and diode junction parasitic capacitances. In this figure, a fourth order model of the transformer has been employed as a model for the non ideal transformer [44]. In the proposed resonant converter, the parallel resonant capacitor in the secondary side of the transformer can merge all parasitic capacitors of the secondary side into the resonant circuit. According to Fig. 7, the proposed topology does not employ any series resonant capacitor in the primary side of the converter, which eliminates the dielectric power loss and facilitates the charger design in terms of component selection. In Fig. 7, all ofthe elements in the secondary side are defined with an apostrophe,but in all equations, the variables and elements are transferred tothe primary side with respect to the transformer turn-ratio, and areshown without an apostrophe. According to Fig. 7, the total amountof parallel capacitance in the secondary of the transformer can be obtained as follows [45]:

$$C_t = C_p + C_{w,s} + C_j$$

In order to model the interaction between the output side (theoutput rectifier, output filter, and load) and the parallel resonant capacitor, the output-side and parallel resonant elements are modeled using an equivalent impedance. The elements of the

International Journal of Research
Available at https://edupediapublications.org/journals
p-ISSN: 2348-6848
e-ISSN: 2348-795X
Volume 06 Issue 13
December 2019

equivalent circuit are defined as follows [37]:

$$R_{eq} = \frac{\sin^2\psi}{\pi C_t \omega_s},\ C_{eq} = \frac{\pi C_t}{\psi - \sin\psi\cos\psi}$$

The angle ψ is the interval during which the output rectifier diodes turn off and the resonant circuit is disconnected from the load (presented in Fig. 6) and is given by:

$$\psi = \cos^{-1}\left(\frac{\pi - 2\omega_s R_L C_t}{\pi + 2\omega_s R_L C_t}\right)$$

Fig. 8 shows the AC equivalent circuit of the resonant circuit along with the equivalent impedance of the transformer secondary side. By using this equivalent circuit, it is possible to employ the nFHA technique for analysis of the L3C resonant circuit. In order to calculate the output current, the second series resonant inductor current is considered purely sinusoidal. Due to the non-conduction angle of the output rectifier, the output current and output voltage can be obtained as follows:

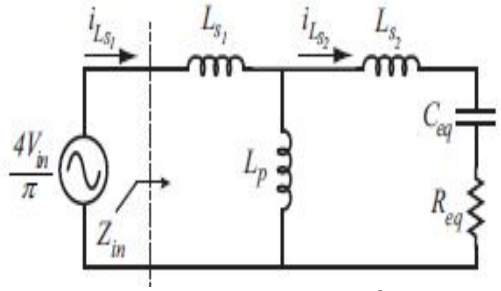

Fig. 8. AC equivalent circuit of the L3C resonant converter.

$$I_o = \frac{1}{2\pi}\left(\int_{\psi}^{\pi} i_{Ls_2}\, d(\omega_s t) + \int_{\pi+\psi}^{2\pi} i_{Ls_2}\, d(\omega_s t)\right) = \frac{(1+\cos\psi)}{\pi} I_{Ls_2}$$

$$V_{out} = R_L . I_{out} = R_L \frac{(1+\cos\psi)}{\pi} I_{Ls_2}$$

According to Fig. 8, applying KVL and KCL gives the relation between output voltage and resonant circuit input current.

$$I_{Ls_2} = \left|\frac{j\omega_s L_p}{j\omega_s L_p + j\omega_s L_{s_2} + R_{eq} + \frac{1}{j\omega_s C_{eq}}}\right| I_{Ls_1}$$

In order to calculate the resonant circuit input current, the input impedance of the AC equivalent circuit should be obtained, which can be expressed by:

$$\mathbf{Z_{in}}(j\omega_s) = j\omega_s L_{s_1} + (j\omega_s L_p) \| (j\omega_s L_{s_2} + R_{eq} + \frac{1}{j\omega_s C_{eq}})$$

One of the advantages of the proposed resonant converter is its ability to limit the output current. In this case, the L3C resonant converter can not only provide a constant current for charging the battery pack, but also protect the full-bridge inverter from over current and short circuit conditions. In over-current conditions, Req → 0 and by considering (15), Zin would be as follows:

$$\mathbf{Z_{in}}(j\omega_s) = j\omega_s L_{s_1} + j\omega_s L_p \| j\omega_s L_{s_2}$$

In this case, the inverter switches are loaded by an inductor that can limit the switches current and also load current. In fact, the resonant circuit provides an inherent short circuit protection
at any operating frequency for the full-bridge inverter. In the AC equivalent circuit, the fundamental component of the resonant circuit input voltage (vAB1 (t)) can be obtained as follows:

$$v_{AB_1} = \frac{4V_{in}}{\pi}\sin(\omega_s t)$$

According to Fig. 8 and Eqs. (15) and (17), the amplitude ofI_{Ls1} (MOSFETs current) can be obtained as follows:

$$I_{L_{s1}} = \frac{4V_{in}}{\pi|\mathbf{Z_{in}}(j\omega_s)|}$$

The following normalized parameters are introduced for the resonant circuit.

$$L = L_p + L_{s_2}, L_n = \frac{L_{s_1}}{L_p}, L_s = \frac{L_{s_1}}{L_{s_2}},$$

$$Z_0 = \sqrt{\frac{L}{C_t}}, Q_L = \frac{R_L}{Z_0}, \omega_0 = \frac{1}{\sqrt{LC_t}}, \omega_n = \frac{\omega_s}{\omega_0}$$

Considering Eq. (13), (14), (18) and (19) the normalized voltagegain of the L3C resonant converter is obtained as follows:

International Journal of Research
Available at https://edupediapublications.org/journals
p-ISSN: 2348-6848
e-ISSN: 2348-795X
Volume 06 Issue 13
December 2019

$$M_v = \frac{V_{out}}{V_{in}} = \frac{Q_L Z_0 (1+\cos\psi)}{\pi V_{in}} \cdot \left| \frac{\frac{j\omega_n L_s}{L_n+L_s}}{\frac{\sin^2\psi}{\pi\omega_n} + j\left(\frac{\omega_n L_s}{L_n+L_s} + \frac{\omega_n L_n}{L_n+L_s} - \frac{\psi-\sin\psi\cos\psi}{\pi\omega_n}\right)} \right| \frac{4}{\pi |Z_{in,n}(j\omega_n)|}$$

$$\psi = \cos^{-1}\left(\frac{\pi - 2\omega_0 Q_L}{\pi + 2\omega_0 Q_L}\right)$$

In the next section, Eq. (20) will be employed to study the voltage gain behavior of L3C resonant converter and circuit elements design.

L3C CONTROL STRATEGY FOR PV TO BATTERY APPLICATIONS

In this section, the control block diagram of the L3C resonant converter as a charger for PV to high voltage battery pack will be explained. A Li-Ion battery pack has two different modes in its charging profile, which are constant current and constant voltage modes, and EV on-board battery chargers are designed based on this battery charging profile [46, 47]. During the constant current mode, the battery pack is charged with the maximum allowable charging current until the battery voltage reaches the float voltage. In the constant voltage mode, the battery voltage is regulated at the float voltage (V'_{bat} = 430V) and the charging action continues until the charging current drops to a certain amount of the rated current(e.g. 3%). The power level of the on-board battery charger for EV applications is around 3kW, and depending on the battery pack capacity, the charger can provide 10 to 20A during constant current mode [47, 48]. However, the maximum PV panel power is limited to several hundred watts, which means the charging current is much lower than on-board chargers. Although a maximum charging current is allowed for the Li-Ion battery pack, it is also possible to charge the battery at a lower rate with a longer charging time without reducing the life [49].

Fig. 9(a) presents the charging cycle profile of the high voltage battery pack when the maximum input power is available by the PV panel (P_{pv} = 365W atV_{pv} = 44.5VDC according to Fig. 3(b)) and the battery voltage dropped to its minimum level (V'_{bat} = 230VDC). Since the target for the PV to the battery application is to extract the maximum power from the input, the charging profile can be divided into two main parts, which are constant power mode (MPPT) and constant voltage mode. Considering the input power (Ppv) equal to 365Wand an average efficiency of 96% for the resonant power converter, the transferred power to the battery by the resonant converter will be 350W. During the first stage of the charge, the battery voltage increases from its minimum level to the charge float voltage and the output power is constant; therefore, the charging current slowly decreases from 1.5A to 0.8A, as shown in Fig. 9(a). In the second stage, the battery voltage is regulated at the float voltage until the battery is fully charged. Fig. 9(b) shows operating trajectories ofthe L3C resonant converter during different states of charge. The details of each trajectory are presented as follows:

1): The starting switching frequency of the L3C resonant converter is set to be the maximum value. Starting from f_s = 400kHz,the output voltage is less than 230VDC, and the converter works under no-load condition. In this case, the controller decreases the switching frequency until the output voltage reaches the battery voltage (V'_{bat} = 230VDC).

2): When the output voltage reaches to 230VDC, the battery pack starts to sink the charging current. At this stage, the MPPTalgorithm kicks in and, by decreasing the switching frequency, the maximum power is extracted from the PV panel. Finally, the operating point of the converter

will be settled in V'_{bat} = 230VDCand I'_{bat} = 1.5ADC.

3) and 4) : According to Fig. 9(a), during each state of charge the battery pack has different voltage and current levels, and therefore behaves similar to a variable resistor. Starting fromV'bat = 230VDC to V'bat = 430VDC, Fig. 9(b) presents three voltage gain curves of the L3C resonant converter when the maximum power is transferred to the battery pack (gray, red, and yellow curves). During these states, the MPPT algorithm is looking for maximum power from the PV panel and adjusts the switching frequency accordingly. In this stage, the charging current decreases from 1.5ADC to 0.8ADC.

5) and 6) : When the battery voltage reaches 430VDC, the battery state of charge enters constant voltage mode. In this stage, the voltage control loop kicks in and regulates the battery voltage at the float voltage by increasing the switching frequency. When the charging current drops to a predefined value (e.g. 3%), the battery charger enters to standby mode. Fig. 9(c) demonstrates the control block diagram, which is employed for the L3C resonant converter for PV to high voltage battery pack applications. As mentioned, the control scheme consists of the MPPT algorithm and voltage loop, which are responsible for extracting the maximum power from PV panel and regulating the output voltage at the float level, respectively. As mentioned in Section IV, since the resonant circuit provides an inherent short circuit protection at any operating frequency and limits the maximum output current to 1.5A, the proposed control scheme does not employ any current loop, neither for the output current regulation, nor for the short circuit protection.

RESONANT POWER CONVERTER DESIGN

In this section, the design procedure will be presented for power conditioning of a 350W solar PV panel to high voltage battery pack, using the proposed L3C resonant converter. The main object during design procedure is to design L3C in such a way as to cover all regions of the Power-Voltage plane presented in Fig. 1(b)(V_{pv} = 24−45VDC), while responding to battery different states of charge (V_{out} = 230 − 430VDC and I_{out} = 0 − 1.5ADC).According to the steady-state analysis of the L3C resonant converter, the voltage gain equation, obtained for L3C steady state

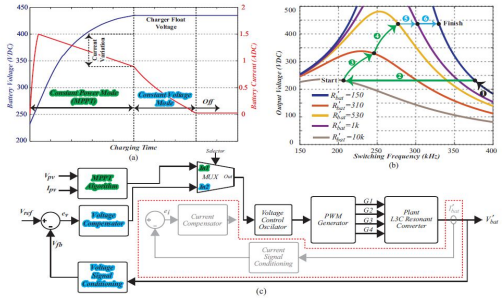

Fig. 9. a) The charging cycle profile for a high voltage battery pack by considering the constant power mode (MPPT) for the PV panel and constant voltage mode during the charger float voltage, b) The L3C battery charger trajectory for different states of charge, and c) The L3C control loop blockdiagram for PV to battery applications. (Due to the inherent current limit capability of the L3C resonant power converter, the current control loop (blocksinside the red dashed line) is eliminated from the control scheme.

condition, is a function of four normalized variables (L_n, L_s, Q_L,and ω_n). The desired normalized parameters should be selectedin such a way to provide essential voltage gain for boosting thevoltage from PV panel to high voltage battery while providing soft switching conditions for all semiconductor devices. Fig. 10 presents the voltage transfer function M_v versus normalized frequency for L_n = 0.25, L_s = 5, Q_L = 2 as the normalized parameters. In this case, Q_L = 2 presents the load condition related to the

International Journal of Research
Available at https://edupediapublications.org/journals
p-ISSN: 2348-6848
e-ISSN: 2348-795X
Volume 06 Issue 13
December 2019

maximum output voltage and output power, V_{out} = 430VDCand P_{out} = 350VDC at the minimum surface temperature and maximum irradiance (−20°C and 1000W/m^2). The main specifications of the battery charger are presented in Table I. According to Table I, the based resonant frequency is equal tof_0 = 140kHz. By choosing ω_n= 2, the switching frequency is calculated as:

$$f_0 = 140kHz,\ f_n = 2,\ f_n = \frac{f_s}{f_0} \implies f_s = 280kHz$$

The voltage gain at f_n = 2 (brown curve, Q_L = 2) for the nominal load conditions are given as follows:

$$M_v = 2.2\ for\ Q_L = 2,\ L_n = 0.25,\ L_s = 5$$

Therefore, the parallel resonant capacitor voltage (output voltage)and transformer turns-ratio are calculated as follows:

$$V_{out,n} = M_v.V_{in} = 2.2 * 44.5 = 98V\,DC,$$
$$n = \frac{N_p}{N_s} = \frac{V_{out,n}}{V'_{out,n}} \implies n = \frac{98}{430} = 0.23$$

According to Eq. (19), the characteristic impedance and resonance frequency are given by:

$$Z_0 = \frac{{V_{out}}^2}{P_{out}Q_L} = 13.8\Omega,\ \omega_0 = \frac{\omega_s}{\omega_n} = 280\pi e^3$$

Therefore, the resonant components are obtained as follows:

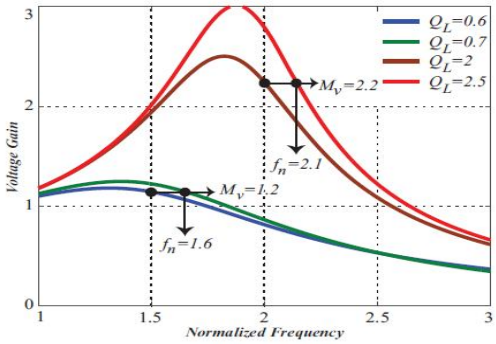

Fig. 10. Magnitude of voltage transfer function (M_v), using the voltagegain equation of the L3C resonant converter for L_n = 0.25, and L_s = 5,with constant values for normalized load resistances (Q_L).

TABLE I
L3C PROTOTYPE PLATFORM PARAMETERS

Parameters	Value
Input Voltage, V_{in}	$24 - 45V\,DC$
Output Voltage, $V'_{out,n}$	$230 - 430V\,DC$
Maximum Output Power, P_{out}	$350W$
Switching Frequency Range, f_s	$180 - 400kHz$
Based Resonant Frequency, f_0	$140kHz$
First Series Resonant Inductance, L_{s_1}	$3.75\mu H$
Second Series Resonant Inductance, L_{s_2}	$0.7\mu H$
Parallel Resonant Inductance, L_p	$15\mu H$
Parallel Resonant Capacitance, C'_p	$5nF$
Transformer Turn's Ratio, $n = \frac{N_p}{N_s}$	$4:18$

$$L = \frac{Z_0}{\omega_0} = 15.7\mu H,\ C_p = \frac{1}{Z_0.\omega_0} = 82nF,$$
$$L_{s_1} = 3.75\mu H,\ L_p = 15\mu H,\ L_{s_2} = 0.7\mu H$$

The L3C resonant circuit parameters used in the experimental prototype are summarized in Table I.

EXPERIMENTAL RESULTS AND THEORY VALIDATION

In order to investigate the performance of the proposed fourth order L3C resonant converter, a prototype platform has been employed to extract the maximum obtainable coverage of Fig. 1(b) under different output voltage and current conditions. The test setup picture is presented in Fig.11. According to Table I, the switching frequency range is between 180 and 350kHz, and the frequency for maximum output power at maximum output voltage set to be 280kHz.

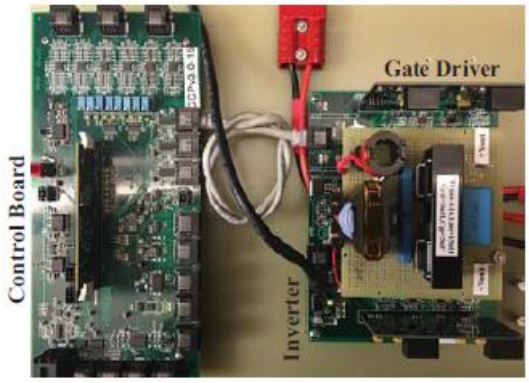

Fig. 11. Prototype test platform of the L3C resonant power converter.

Due to high current amplitude in the primary side, a high efficiency full-bridge

inverter with low on-resistance MOSFET(2.5 mOhm) is used to convert the input DC voltage toa high-frequency AC voltage. The resonant tank consists ofan external air-core inductor (L_{ext} = 3.1μH placed in series with the transformer's primary side), an external parallel capacitor (placed in the secondary side of the transformer),and the parasitic components of the transformer (including primary and secondary leakage inductances and magnetizing inductance). In order to investigate the power converter performance, the power platform was tested under different input-output scenarios, and Fig. 12 shows the experimental results for the minimum and maximum output voltage under different input voltage and maximum available power conditions. Each figure contains of full-bridge inverter voltage, resonant circuit current, transformer secondary side voltage, and transformer secondary side current.

The experimental results show the response of the L3Cresonant converter to input-output voltage variations, which caused as a result of either changing in the PV panel, or battery state of charge. As mentioned in the introduction, the battery charger must be able to respond to different modes of the charge algorithms and track the input voltage variation in order to transfer the maximum available power. According to extracted experimental results, the proposed fourth orderL3C resonant converter can regulate the output voltage and current over a wide range (V'_{bat} = 230 − 430VDC and I'_{bat} = 0− 1.5ADC), and track the input voltage variation in order to extract the maximum available power from PVpanel, using the switching frequency modulation. In order to provide soft switching conditions for power MOSFETs, the phase angle of input impedance should be positive. In other words, the input resonant circuit current should remain lagging the full-bridge inverter voltage. According to experimental results, the zero crossings of the resonant circuit input current are within the inverter output voltage pulse and, as a result, in all of the conditions described, the full-bridge switches are fully turned on under zero voltage.

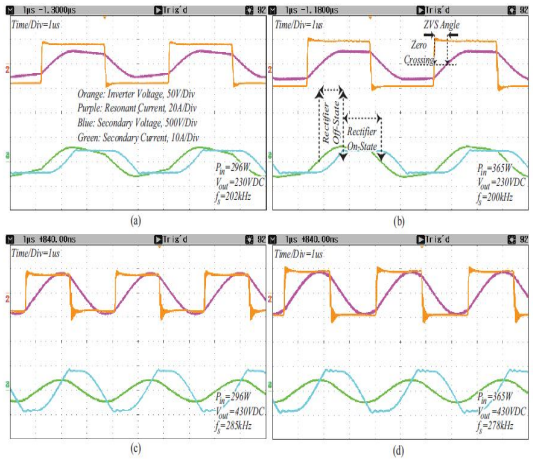

Fig. 12. Experimental results of fourth order L3C resonant converter platform under different PV panel conditions and minimum-maximum output voltage, a) 1000W/m^2 at 25°C, b) 1000W/m^2 at −20°C, c) 1000W/m^2 at 25°C, and d) 1000W/m^2 at −20°C.

On the other hand, to provide a high-quality output voltage and maximize the converter efficiency, it is vital to realize soft commutation for the output rectifier diodes. Basically, the reverse recovery current of output rectifier diodes during the turn-off transition leads to high voltage peak across output diodes and as a result, diodes with more withstand voltage should be selected, which means more conduction losses. Experimental results presented in Fig. 12 include the experimental waveforms of voltage and current on the secondary side of the transformer in theL3C resonant converters. According to these figures, ZCS is provided for output rectifier diodes, and voltage peak is eliminated. As indicated in experimental figures, in the end of power transfer interval, once the transformer secondary current reaches zero, the output

diodes current smoothly reaches zero. This causes ZCS at turn-off and avoids any reverse recovery losses in the output diodes. In addition, the voltage across the diodes is smooth and sinusoidal during the switching transitions which leads to the minimum negative impact of the diode junction capacitance in transient time. As mentioned in Section IV and presented in Fig. 7, there is not any series capacitor in the L3C resonant topology. There is a chance that series capacitor elimination along with no similarity of full bridge gate signals leads to DC current offset of the resonant current and transformer saturation. However, due to the small air gap of the transformer between its ferrite cores for the magnetizing inductance adjustment, the transformer saturation can be prevented. Experimental results show that in all presented conditions, the resonant current has no DC offset and the transformer operates without any saturation.

Experimental results related to over current and short-circuit conditions demonstrate the ability of the proposed converter in terms of output current limitation during overload conditions. Fig. 13 presents a worst-case scenario where the converter operates in output short circuit and maximum input voltage conditions. According to this figure, the converter can safely work in this situation and limit the output current by I'_{out} = 1.5ADC. Fig. 14 presents the efficiency curves for different input PV panel voltages and output battery conditions. Each experimental point in this figure is related to one maximum power point, presented in Fig. 3. According to these curves, the resonant converters designed for this study present a maximum efficiency equal to 97.5%. Fig. 14(a) shows the converter efficiency is above92% from full load to 50% of the load, but due to the circulating current in light load condition, the converter efficiency decreases at light loading conditions

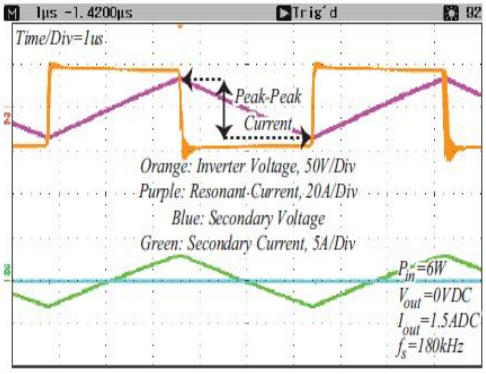

Fig. 13. L3C resonant converter short circuit test at minimum switching frequency (f_s = 180kHz) and maximum input voltage (V_{in} = 44VDC).

CONCLUSION

This paper introduced the L3C resonant power converter with extreme regulation capability, which can be employed for solar battery charger applications. The main advantages of the proposed resonant converter are its ability to respond to different battery states of charge, while tracking the input voltage variations of the PV panel, which occur as a result of changes to the maximum power point. The proposed converter has the voltage gain of more than two, which contributes to the required voltage gain for boosting the input voltage to a high voltage one. Also, the L3C topology can provide an inherent over-current protection, which can control the battery current during constant current mode and simplifies the control and protection circuit design. In addition, soft switching of semiconductor devices provides high efficiency, and the capability of working in high switching frequency. The complete analysis of the resonant converter along with mathematical equations were presented. The experimental results verify the theoretical analysis and the performance of the proposed converter in terms of tracking the input voltage for maximum

power extraction and operating under different output voltage and current conditions.

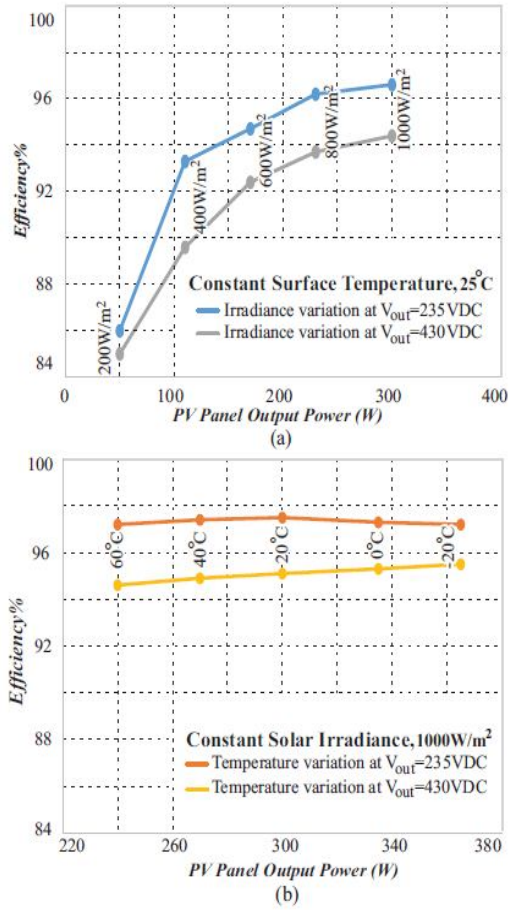

Fig. 14. Efficiency curves of the L3C resonant converter for different conditions, a) Blue and gray lines present efficiency for constant surface temperature (25◦C) and irradiance variations at V_{out} = 235VDC and V_{out} = 430VDC, respectively, and b) Orange and yellow lines present efficiency for constant solar irradiance (1000W/m^2) and temperature variations at V_{out} = 235VDC and V_{out} = 430VDC, respectively.

REFERENCES

[1] S. Arshadi, B. Poorali, E. Adib, and H. Farzanehfard, "High step-up DC-AC inverter suitable for AC module applications," IEEE Trans- action on Industrial Electronics, vol. 63, no. 11, pp. 832-839, May.2017.

[2] R.Ahrabi, H.Ardi, M.Elmi, A.Ajami, "A novel step-up multi- input DC-DC converter for hybrid electric vehicles application," IEEE Transaction on Power Electronics, vol. 32, no. 5, pp. 3549-3561, Nov.2016.

[3] U. R. Prasanna, A. K. Singh, and K. Rajashekara, "Novel bidirectional single-phase single-stage isolated AC-DC converter with PFC for charging of electric vehicles," IEEE Transaction on Transportation Electrification, Early Access 2017.

4] P.He, and A.Khaligh, "Comprehensive analyses and comparison of 1kWisolatedDCDCconverters for bidirectional EV charging systems," IEEETransactiononTransportationElectrification,vol.3,no.1,pp. 147-156,Mar.2017.

[5] VIAMotorsInc., SlTRUX Solar Cover for the 2014VIAVTRUX, www.viamotors.com/vehicles/soltrux

[6] University of Michigan's solar racing team, "Sun kings cross the outback[solarpoweredvehiclesmarathon], " IEEESpectrum,vol.39, no.2,pp.40-46,Feb.2002.

[7] M.I.Shahzad, S.Iqbal,andS.Taib, "A wideout putrange HB-2LLC resonantconverterwith hybridrectifierfor PEVbatterycharging," IEEETransactiononTransportationElectrification,vol.3,no.2,pp. 520-531,Jun.2017.

[8] F.Musavi, M.Craciun, D.Gautam, W.Eberle, and W.Dunford, "An LLCresonant DC-DC converter for wide output voltage range battery charging applications," IEEE Transaction on Power Electronics,vol. 28,no.12,pp.5437-5445,Dec.2013.

[9] M.Das, and V.Agarwal, "Design and analysis of a high-efficiency DC-DC converter with soft switching capability for renewable energy applications requiring high voltage gain," IEEE Transaction on Industrial Electronics,vol.63,no.5,pp.2936-2944,May.2016.

[10] L.Muller ,and J.Kimball,"High gain DC-DC converter based on the Cockcroft-Waltonmultiplier,"IEEETransactiononPowerElectronics, vol.31,no.9,pp.6405-6415,Sep.2016.

[11] W.Li,andX.He,"Reviewofnon-isolated high-step-up DC/DCconvertersinphotovoltaicgrid-connectedapplications," IEEETransactiononIndustrialElectronics,vol.58,no.4,pp.1239-1250,Apr.2011.

[12] G.Wu,X. Ruan,andZ. Ye,"Non-isolatedhighstep-upDC-DC convertersadoptingswitched-capacitor cell,"IEEETransactionon IndustrialElectronics,vol.62,no.1,pp.383-393,Jan.2015.

[13]Y.Tang, D.Fu, T.Wang, and Z.Xu "Hybrid switched-inductor converters for high step-up conversion," IEEE Transactionon Industrial Electronics, vol.62,no.3,pp.1480-1490,Mar.2015.

[14] Underwrites Laboratories Inc., UL60950: Safety of information tech-nologyequipment,Thirdedition,2000.

[15] Underwrites Laboratories Inc., UL1741: Inverters, converters, controllers and interconnection system equipment for use with distributed energy resources, 2010.

[16] X.Hu and C.Gong, "A high-efficiency flyback micro-inverter with a new adaptivesnubber for photo voltaic applications," IEEE Transaction on Power Electronics,vol.31,no.1,pp.318-327,Jan.2016.

[17] Y.Shi, R.Li, Y.Xue, and H.Li, "Optimized operation of current-feddualactivebridgeDC-0DCconverterforPVapplications," IEEE Transaction onIndustrialElectronics, vol.62,no.11,pp.6986-6995, Nov.2015.

[18] F.Evran,andM.Aydemir, "Isolated highstep-upDC-DCconverter withlowvoltagestress,"IEEETransactionoPowerElectronics,vol.29,no.7,pp.3591-3603,Jul.2014.

[19]M.Cacciato, A.Consoli,R.Attanasio, and F.Gennaro,"Soft- switching converter with HF transformer for grid-connected photo- voltaicsystems, " IEEE Transaction onIndustrialElectronics,vol.57, no.5,pp.1678-1686,May2010.

[20]W.Cha, Y.Cho,J.Kwon,andB.Kwon,"Highly efficient mi- croinverterwithsoft-switching step-upconverterandsingle-switch-modulationinverter,"IEEETransactiononIndustrialElectronics,vol.62,no.6,pp.3516-3523,Jun.2015.

[21] F.Shang,H. Wu,G. Niu,M. Krishnamurthy, and A. Isurin, "Dynamic analysis and control approach for a high gain step-upconverter for electrified transportation," IEEE Transaction on Transportation Electrification, Early Access 2017.

[22] F.Shang, G.Niu, and M.Krishnamurthy, "Designandanalysisofa high-voltage-gain step-upresonant DCDC converter for transportation applications," IEEETransaction onTransportationElectrification,vol.3,no.1,pp.157-167,Mar.2017.

[23] Y.Kim, S. Shin,J. Lee, Y.Jung,andC. Won,"Soft-switchingcurrent- fed pushpull converterfor 250-W AC module applications,"IEEE TransactiononPowerElectronics,vol.29,no.2,pp.863-872,Feb.2014.

[24] H.Hu, X.Fang, F.Chen, Z.Shen, and I.Batarseh, "A Modified high- efficiency LLC converter with two transformers for wide input-voltage range applications," IEEETransactiononPowerElectronics,vol.28, no.4,pp.1946-1960,Apr.2013.

[25] T.Jiang,J.Zhang, X.Wu,K.Sheng, andY.Wang, "Abidirectional LLCresonantconverter withautomatic forward and backward mode transition,"

IEEE Transaction on Power Electronics, vol.30,no.2,pp.757-770,Aug.2014.

[26] N. Shafiei, M. Ordonez, C. Botting, M.Craciun, and M.Edington, "FourthorderL3Cresonantconverter for wide output voltage regulation," inproc. IEEE Applied Power Electronics Conference and Exposition(APEC),2015,pp.1467-1471.

[27]T.LaBella, and J.Lai, "A hybrid resonant converter utilizing a bidirectional GaNAC switch for high-efficiencyPV applications," IEEETransactiononIndustryApplication,vol.50,no.5,pp.3468-3475,Sep.2014.

[28] D.Vinnikov, A.Chub, E.Liivik,I.Roasto, "High-performance quasi- Z-source series resonant DC-DC converter for photovoltaic module level power electronics applications," IEEE Transaction on PowerElectronics,Early Access,2016.

[29]T.Hongmei, F.Mancilla David, K.Ellis, E.Muljadi, A detailed performance model for photovoltaic systems, National Renewable Energy Laboratory, USANREL/JA-5500-54601,July2012

[30] G.M.Masters, Renewable and Efficient Electric Power Systems, John WileyandSons, NY,2004.

[31] A.D. Rajapakse, D.Muthumuni, "Simulation tools for photovoltaic system grid integration studies," inproc. IEEE Electrical Power and Energy Conference(EPEC),2009,pp.1-5.

[32] S.Kim, J.Jeon, C.Cho, E.Kim, J.Ahn, "Modeling and simulation of a grid-connected PV generation system for electromagnetic transient analysis, "ElsevirSolarenergy,vol.83,no.5,pp.664-678,May2009.

[33] Canadian Solar Inc., MAX POWER CS6X-310P, http://www.canadiansolar.com/na/solar-panels/maxpower.html

[34] M.K.KazimierczukandD.Czarkowski, Resonantpowerconverters, JohnWileyandSons,NY,1995.

[35] N.Shafiei, M.Pahlevaninezhad, H.Farzanehfard, A.Bakhshaei, and P.Jain,"Analysisofafifth-order resonant converter for high-voltage DC powersupplies," IEEE Transaction on Power Electronics, vol.28, no.1,pp.85-100,Jan.2013.

[36] N.Shafiei, and M.Ordonez, "Improving the regulation range of EV batterychargerswithL3C2resonantconverters,"IEEETransaction onPowerElectronics,vol.30,no.6,pp.3166-3184,Jun.2015.

[37] Y.A.Ang, C.M.Bingham, M.P.Foster, D.A.Stone and D.Howe, "Design oriented analysis of fourth-order LCLC converters with capacitive outputfilter", Inst.Elect.Eng. Electric Power Applications, vol.152,no.2,pp.310-322, Mar.2005.

[38] J.Biela, U.Badstuebner and J.W.Kolar, "Designofa5-kW,1-U,10-kW/dm3 resonant DC-DC converter for telecom applications,"IEEE TransactiononPowerElectronics,vol.24,no.7,pp.1701-1710,Jul. 2009.

[39] J.A.M. Ramos, A.M. Pernia, J.Diaz, F.Nuno and J.A.Martinez, "Power supply forahigh-voltage application," IEEETransaction on PowerElectronics,vol.23,no.4,pp.1608-1619,Jul.2008.

[40] M.A.Saket, N.Shafiei, M.Ordonez, "LLC Converters with Planar Transformers: Issues and Mitigation," IEEE Transaction on Power Electronics,vol.32,no.6,pp.4524-4542,Jun.2017.

[41] M.A.Saket,N.Shafiei,M.Ordonez, "Low Parasitics Planar Trans- former for LLC Resonant Battery Chargers," inproc. IEEE Applied Power Electronics Conference and Exposition (APEC),2016,pp.854-858.

[42] N.Shafiei, M.Ordonez, M.Craciun, C.Botting, and M.Edington, "Burst Mode Elimination in High-Power LLC Resonant Battery Charger for Electric Vehicles," IEEE Transactionon Power Electronics, vol.31,no.2,pp.1173-1188,Feb.2016.

[43]H.Choi and FPS Application Group, Half-bridge LLC resonant converter design using FSFR-series Fair child power switch, Fairchild semiconductor corporation, Rev.1.0.010/9/07,2007.

[44] D.Bortis, J.Biela, G.Ortiz and J.W.Kolar, "Design procedure for compact pulse transformers with rectangular pulse shape and fast rise times,"IEEETransactiononDielectricandElectricalInsulation,vol.18,no.4,pp.1171-1180,Aug.2011.

[45] B.Lee, M.Kim, C.Kim, K.Park, andG. Moon, "Analysis of LLC resonant converter considering effects of parasitic components," Telecommunications Energy Conference,2009,pp.1-5.

[46] Z.Fang, T.Cai, S.Duan, and C.Chen, "Optimal design methodology for LLC resonant converter in battery charging applications based on time-weighted average efficiency," IEEE Transaction on Power Electronics, vol.30,no.10, pp.5469-5483,Oct.2015.

[47] Z.Fang, T.Cai, S.Duan, and C.Chen, "Design methodology of LLC resonant converters for electric vehicle battery chargers," IEEE Transaction on Vehicular Technology, vol.63, no.4,pp.1581-1592, May.2014.

[48] M. Pahle vaninezhad, P.Das, J.Drobnik, P.Jain, and A. Bakhshai, "A novelZVZCSfull-ridgeDC/DC converter used for electric vehicles," IEEETransactiononPowerElectronics,vol. 27,no.6,pp.2752-2769, Jun.2012.

[49] Texas Instruments, Battery charging, Literaturenumber:SNVA557,2011.